



Contents lists available at ScienceDirect

Surface & Coatings Technology

journal homepage: www.elsevier.com/locate/surfcoat

Evolution of the thermal conductivity of arc evaporated fcc-Ti_{1-x-y}Al_xTa_yN coatings with increasing Ta content

Helene Waldl^{a,*}, Michael Tkadletz^b, Markus Winkler^c, Birgit Grossmann^d, Christoph Czettl^e, Markus Pohler^e, Nina Schalk^a

^a Christian Doppler Laboratory of Advanced Coated Cutting Tools, Montanuniversität Leoben, Franz Josef-Straße 18, 8700 Leoben, Austria

^b Department of Materials Science, Montanuniversität Leoben, Franz Josef-Straße 18, 8700 Leoben, Austria

^c Department Thermal Energy Converters, Fraunhofer Institute for Physical Measurement Techniques IPM, Heidenhofstraße 8, 79110 Freiburg, Germany

^d voestalpine BÖHLER Edelstahl GmbH & Co KG, Mariazeller-Straße 25, 8605 Kapfenberg, Austria

^e CERATIZIT Austria GmbH, Metallwerk-Plansee-Straße 71, 6600 Reutte, Austria

ARTICLE INFO

Keywords:

PVD

Hard coatings

TiAlTaN

TDTR

Thermal conductivity

ABSTRACT

Hard coatings are commonly applied in severe cutting applications, where significant heat is generated. Thus, their thermal conductivity should be kept low to provide a heat barrier to the substrate and consequently to increase the service life time of the tools. Although, Ti_{1-x-y}Al_xTa_yN protective coatings have been applied successfully in the cutting industry, their thermal conductivity is barely investigated. The focus of this study is to determine the thermal conductivity of face-centered cubic (fcc)-Ti_{1-x-y}Al_xTa_yN coatings with a Ti/Al ratio of 1:1 and a Ta content increasing from 0 up to 23 at.%. The investigated coatings were deposited by cathodic arc evaporation to a coating thickness of 3.2 μm ± 0.4 μm. The microstructure and chemical composition were studied using X-ray diffraction and energy dispersive X-ray spectroscopy, respectively. Time-domain thermoreflectance measurements revealed a low thermal conductivity for fcc-Ti_{1-x}Al_xN with 5.7 W/(mK) and a further decrease with increasing Ta content to 2.4 W/(mK) for 23 at.% Ta. This trend can be explained by the small grain size caused by the Al addition leading to increased boundary scattering and the incorporation of Al and larger Ta atoms in the fcc-TiN lattice resulting additionally in alloy scattering, as the thermal conductivity decreases with increasing phonon scattering processes.

1. Introduction

Current trends in the cutting industry continue towards higher productivity and simultaneous longer service lifetime of tools. Therefore even well-established coating systems, like Ti_{1-x}Al_xN, need to be further improved [1–4]. The addition of a fourth element to this system is one possible approach. Suitable candidates are for example Cr, Y, V or Ta, [1,5–8]. Especially Ti_{1-x-y}Al_xTa_yN is widely applied due to its superior mechanical and tribological properties, thermal stability and oxidation behavior compared to the ternary system [8–18]. Since during application high temperatures in the work piece and the tool material can be reached, knowledge about the thermo-physical properties of the respective coating system is essential [19,20]. The thermal conductivity describes the ability of heat dissipation of a material [21]. A low thermal conductivity is supposed to be favorable for hard coatings in cutting processes, since they consequently provide a thermal barrier to the

substrate [22]. The heat is deflected into the chip and thus the thermal loads in the tool are reduced, resulting in a delay or even prevention of plastic deformation of the tool [23]. For dielectric coatings like Ti_{1-x}Al_xN the electronic contribution to the thermal conductivity can be neglected as the phonons are the major heat carriers [24]. Thus, a promising concept for decreasing the thermal conductivity is the combination of phonon scattering processes, like boundary scattering and alloy scattering, due to small grain sizes and large substitutional atoms [25]. Investigations of the thermal conductivity of Ti_{1-x}Al_xN coatings showed a decrease of conductivity with increasing Al content due to grain refinement and the incorporation of Al in the fcc-TiN lattice [26–28]. Also the behavior of the thermal conductivity of Ti_{1-x}Al_xN coatings with increasing temperature has been studied and revealed an increase of the conductivity with increasing temperature resulting from grain coarsening and spinodal decomposition [24,29,30]. Tkadletz et al. investigated the thermal conductivity of a Ti_{1-x-y}Al_xTa_yN coating as a function

* Corresponding author.

E-mail address: helene.waldl@unileoben.ac.at (H. Waldl).

<https://doi.org/10.1016/j.surfcoat.2020.126658>

Received 8 September 2020; Received in revised form 16 November 2020; Accepted 18 November 2020

Available online 19 November 2020

0257-8972/© 2020 The Authors.

Published by Elsevier B.V. This is an open access article under the CC BY-NC-ND license

(<http://creativecommons.org/licenses/by-nc-nd/4.0/>).

of the annealing temperature [21], showing the same trend as observed for $\text{Ti}_{1-x}\text{Al}_x\text{N}$ [24,29,30]. However, literature on the thermal conductivity of the $\text{Ti}_{1-x-y}\text{Al}_x\text{Ta}_y\text{N}$ coating system is rare and to our knowledge no systematic study of the thermal conductivity as a function of the Ta content is available.

Thus, the aim of this work is to investigate the influence of the Ta content on the thermal conductivity of face-centered cubic (fcc)- $\text{Ti}_{1-x-y}\text{Al}_x\text{Ta}_y\text{N}$ coatings with constant Ti/Al ratios and Ta contents in the target between 0 and 15 at.%, which have already been extensively studied with respect to their microstructure, mechanical and thermal as well as oxidation stability in two previous works [13,14]. The thermal conductivity was determined by time-domain thermoreflectance (TDTR) measurements.

2. Experimental

The fcc- $\text{Ti}_{1-x-y}\text{Al}_x\text{Ta}_y\text{N}$ coatings were synthesized using cathodic arc evaporation (CAE), in an industrial scale Oerlikon Balzers Innova deposition plant utilizing powder metallurgically produced targets from Plansee SE with a purity of 99.7% for a Ti/Al atomic ratio of 1:1 and Ta contents of 0 to 1, 2.5, 5, 10 and 15 at.%. The cemented carbide (CC) substrates (SNUN 120312EN geometry, according to ISO 1823), containing 92 wt% WC, 6 wt% Co and 2 wt% mixed carbides, were mounted on the carousel to undergo 3-fold rotation. After plasma etching of the substrates using Ar^+ ions, the depositions were performed in pure nitrogen atmosphere, applying a substrate temperature of 550 °C.

A field emission gun SEM of type Zeiss Auriga was used to investigate the cross-sections of the coatings prepared by ion milling. The chemical composition was determined by EDS at different positions of the coating surface, applying an Oxford Instruments INCA extension, mounted on a Zeiss EVO50 SEM. The microstructure of the fcc- $\text{Ti}_{1-x-y}\text{Al}_x\text{Ta}_y\text{N}$ coatings was investigated utilizing a Bruker AXS D8 Advance diffractometer in grazing incidence geometry (incidence angle 2°), using $\text{Cu-K}\alpha$ radiation with a wavelength of 1.5418 Å. Evaluation of the XRD data was done by Rietveld refinement, where the instrumental broadening was corrected with the measured data of a LaB_6 standard (NIST 660c [31]). A Rigaku Smartlab X-Ray diffractometer and the $\sin^2\psi$ method were applied to evaluate the residual stresses [32].

TDTR was used to determine the thermal conductivity of the different fcc- $\text{Ti}_{1-x-y}\text{Al}_x\text{Ta}_y\text{N}$ coatings. Laser pulses with a pulse duration of 500 fs, a pulse repetition rate of 80 MHz, a wavelength of 785 nm and

an average laser power of 28 mW were generated by the Ti:Sapphire laser system Mai Tai from Spectra-Physics. The pump beam modulation frequency was set to 10.7 MHz. The time delay between pump and probe beam was in the range of 0 to 3600 ps. Prior to measurements, 70 nm of pure Al were deposited using electron beam evaporation to serve as transducer layer. To validate the measurement system, two reference samples, a pure Si wafer and an oxidized one, were analyzed right before the measurements. More details to the TDTR measurements can be found in ref. [33].

3. Results and discussion

The thickness of all investigated coatings is in the range of $3.2 \mu\text{m} \pm 0.4 \mu\text{m}$, as determined from SEM cross-section images. The compositions of the metallic components of the coatings investigated by EDS are shown in Fig. 1 as a function of the composition of the targets. The dashed line indicates an equal composition of target and coating. In Fig. 1a it can be seen that the Ta content is significantly higher in the coatings than in the respective targets. While the highest Ta content in the target is $y = 0.15$, it reaches 0.23 in the coatings. The Ti content in the coating is also slightly higher than in the target, but with increasing Ta content the deviation decreases, as shown in Fig. 1b. The increased Ta and Ti contents in the coatings are compensated by a loss of Al in the coatings compared to the target composition, as visible in Fig. 1c. The lower Al content and the higher Ta and Ti content in the coatings can be explained by the mass difference of these elements. The considerably lighter Al experiences higher scattering in the gas phase and more pronounced resputtering from the growing film [34]. This has also been reported in earlier studies for the $\text{Ti}_{1-x-y}\text{Al}_x\text{Ta}_y\text{N}$ system [8,13,17]. The nitrogen content in all fcc- $\text{Ti}_{1-x-y}\text{Al}_x\text{Ta}_y\text{N}$ coatings is 48.3 ± 3.3 at. %.

The X-ray diffractograms of the coatings in Fig. 2a are presented with an increasing Ta content from bottom to top. The standard peak positions for fcc-TaN (ICDD 00-049-1283), fcc-TiN (ICDD 00-038-1420) and fcc-AlN (ICDD 00-025-1495) are drawn as dashed lines. In addition, the peak positions of WC (ICDD 03-065-4539), stemming from the CC substrate, are marked by squares. All coatings exhibit a single phase fcc B1 structure. The 200 peak of $\text{Ti}_{1-x}\text{Al}_x\text{N}$ with 0 at. % Ta is located in between the fcc-TiN and fcc-AlN standard peak positions but not exactly in the middle as could be expected from the Ti/Al ratio of 1:1, which can be attributed to compressive residual stress. For all coatings compressive residual stresses were determined, which continuously increase with

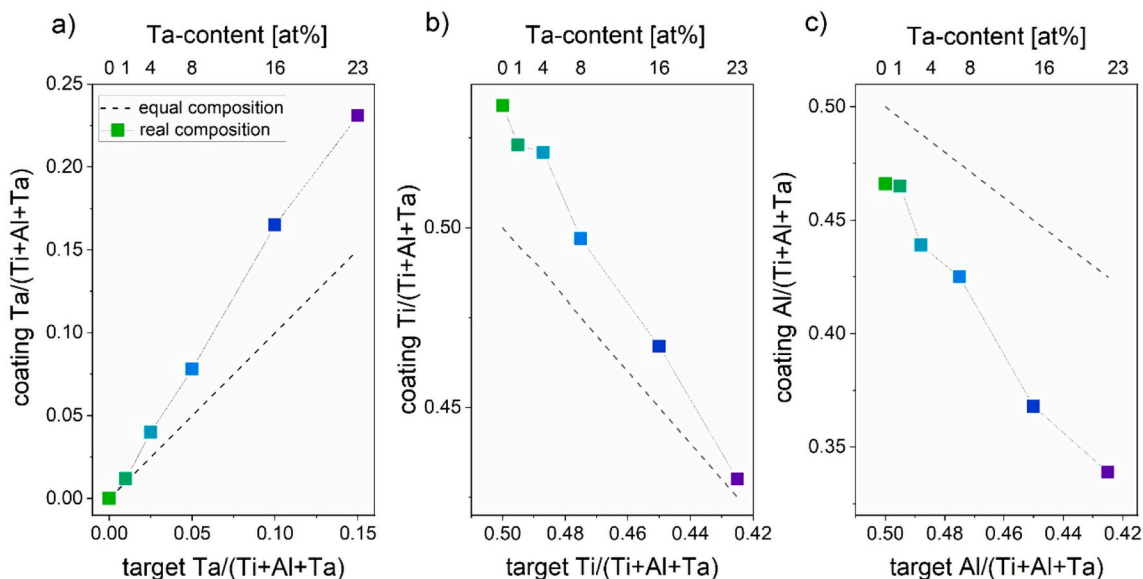


Fig. 1. Composition of the metallic components of the fcc- $\text{Ti}_{1-x-y}\text{Al}_x\text{Ta}_y\text{N}$ coatings as a function of a) the Ta, b) the Ti and c) the Al content in the target, revealing a gain of Ta and Ti and a loss of Al in the coating.

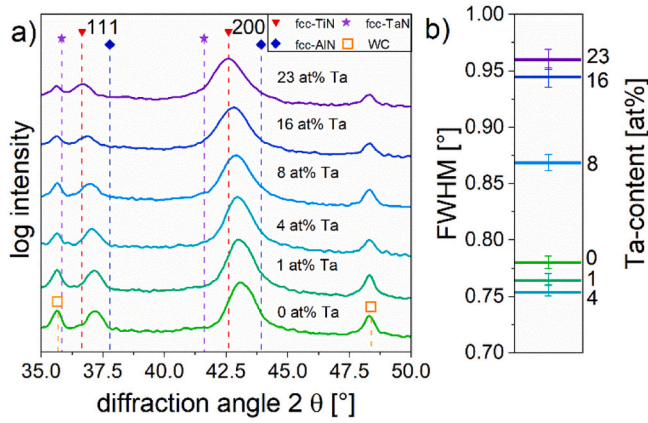


Fig. 2. a) X-ray diffractograms of the fcc-Ti_{1-x-y}Al_xTa_yN coatings and b) the corresponding FWHM.

increasing Ta content from -1.79 ± 0.19 GPa for the fcc-Ti_{1-x}Al_xN coating to -3.31 ± 0.25 GPa for the coating containing 23 at.% Ta, due to more pronounced ion peening during deposition [35,36]. The increasing residual stresses are reflected by a peak shift to even lower diffraction angles with increasing Ta content. In addition, the incorporation of Ta into the fcc-TiAlTa_yN solid solution results in an increase of the lattice parameter, which is confirmed by Rietveld refinement of the respective 200 peaks, evidencing an increase of the lattice parameter from 4.16 ± 0.01 Å for 0 at.% Ta to 4.23 ± 0.02 Å for 23 at.% Ta, and is also reported in earlier studies [8,12,13,17,37]. Further, a peak broadening at Ta contents above 8 at.% is observed, which is also displayed by the trend of the full width at half maxima (FWHM, determined from the 200 peak), shown in Fig. 2b. An increasing FWHM correlates with a smaller size of coherently diffracting domains and/or higher micro strains due to an increased amount of point defects [38,39]. Evaluation of domain size by Rietveld refinement showed a slight decrease from 31 ± 8 nm for 0 at.% Ta to 25 ± 8 nm for 23 at.% Ta. Hereinafter, the determined domain size is assumed as estimate for the grain size [40]. The observed peak broadening is in good agreement with literature [8,13].

SEM cross-section images of three different fcc-Ti_{1-x-y}Al_xTa_yN coatings with Ta contents of 0, 8 and 23 at.% are compared in Fig. 3. These three coatings are representative for the cross-sections of all investigated coatings, showing a dense and fine grained columnar structure in

growing direction. With increasing Ta content the grain size slightly decreases, which is in good agreement with the results of the Rietveld refinement and with literature [8,11].

The thermal conductivity was determined by TDTR. Details of the applied mathematical model which was used to evaluate the TDTR measurements can be found in ref. [33, 41]. Since the thermal penetration depth of the pump beam for fcc-Ti_{1-x}Al_xN has been estimated, according to the equation provided by Cahill et al. [33], to lie within 0.25 and 0.64 μm, the identified coating thicknesses of $3.2 \mu\text{m} \pm 0.4 \mu\text{m}$ are sufficient to ensure that the thermal penetration depth is limited to the coating and does not extend into the CC substrate [33]. To determine the respective thermal conductivity, the heat capacity of the coating is needed as an input parameter for the applied mathematical model. The heat capacity of 2.6 J/(cm³K) for the actual fcc-TiAlN composition was interpolated from values of pure fcc-TiN of 3.14 J/(cm³K) and pure fcc-AlN of 2.39 J/(cm³K) by applying a rule of mixture [42]. Due to a lack of literature, the value for fcc-TaN of 3.51 J/(cm³K) was estimated applying the Dulong-Petit law [43]. Subsequently, the heat capacity for

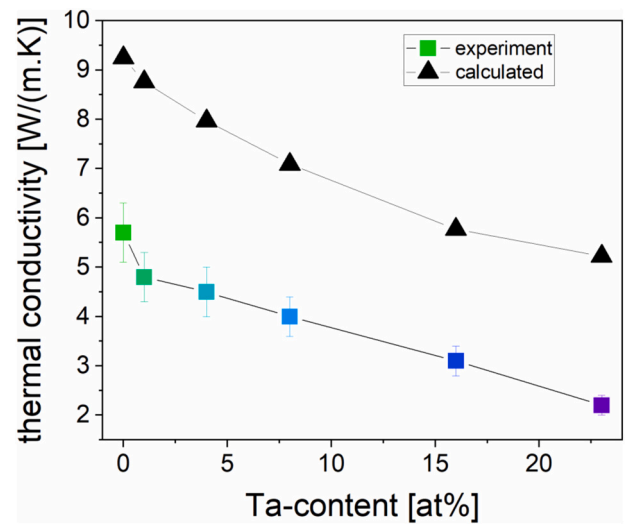


Fig. 4. Thermal conductivity from the TDTR experiment as a function of the Ta content of the fcc-Ti_{1-x-y}Al_xTa_yN coatings indicated by squares. The triangles mark the estimated values for the thermal conductivity, determined using the kinetic model only considering the boundary scattering.

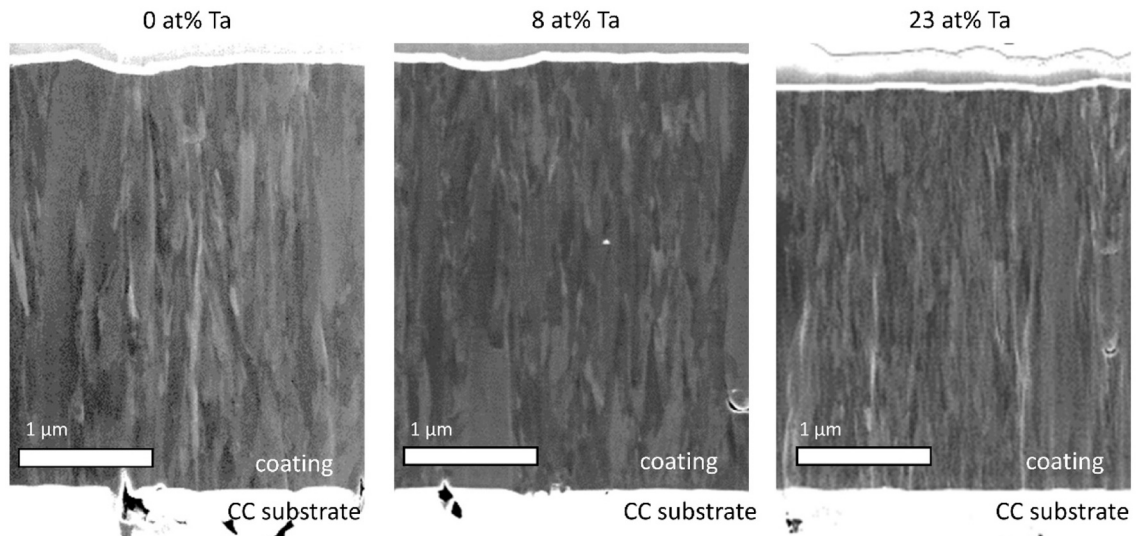


Fig. 3. SEM images of ion-milled cross-sections of three different fcc-Ti_{1-x-y}Al_xTa_yN coatings.

the different fcc-Ti_{1-x-y}Al_xTa_yN coatings was interpolated according to the chemical composition of each individual coating. In Fig. 4 the results of the TDTR measurements are summarized. The thermal conductivity of fcc-Ti_{1-x}Al_xN is 5.7 W/(mK) and in good agreement with earlier studies of comparable coatings [26,28,29]. However, literature values for the thermal conductivity of CAE fcc-TiN and fcc-AlN are 11.9 and 30.0 W/(mK), respectively [44,45]. The considerably lower thermal conductivity of fcc-Ti_{1-x}Al_xN in comparison to the binary materials can be explained by phonon scattering processes, since heat transport in fcc-Ti_{1-x}Al_xN is mainly realized by phonons [25]. Significant phonon scattering caused by a vast number of grain boundaries, due to the small grain size, can reduce the thermal conductivity effectively, as demonstrated in ref. [46]. The grain size of the fcc-Ti_{1-x}Al_xN coating in our study is with ~31 nm considerably smaller than that of the CAE fcc-TiN coating reported by Samani et al. with a columnar grain structure and a grain size of ~94 nm [45]. This grain refinement is in good agreement with literature, evidencing that the incorporation of Al in the fcc-TiN system results in a significant refinement of the grain structure, since the presence of Al atoms effectively prevents the formation of columns [4,28,47,48]. Thus, boundary scattering definitely contributes to the reduction of the thermal conductivity. With increasing Ta content, the thermal conductivity decreases further compared to the fcc-TiAlN coating and it is even lower than the thermal conductivity of pure fcc-TaN with 8.3 W/(mK) [44]. Tkadletz et al. also observed a lower thermal conductivity for fcc-Ti_{1-x-y}Al_xTa_yN compared to fcc-Ti_{1-x}Al_xN [21]. The strongest decline of the thermal conductivity in Fig. 4 can be observed for the first addition of Ta, then it decreases with a constant slope up to a minimum value of 2.4 W/(mK) for 23 at.% of Ta. Using the kinetic model of the thermal conductivity it can be attempted to show the influence of the reduction of the grain size on the thermal conductivity qualitatively. Applying this theory, the thermal conductivity λ can be estimated according to Eq. (1) [49],

$$\lambda = \frac{1}{3} C v^2 \tau, \quad (1)$$

where C is the specific heat capacity, v the average velocity of sound and τ the phonon relaxation time [46,50]. The mean free path of phonons l is the product of the velocity of sound times the phonon relaxation time. For the comparison of the thermal conductivity of coatings with different grain sizes we assume a ballistic phonon transport as simplification. Hence, the mean free path l equals the average grain size [49]. By inserting the values for the different grain sizes, determined by Rietveld refinement, in Eq. (1), the thermal conductivity with increasing Ta content can be estimated. The velocity of sound was assessed with the square root of the Young's modulus, gained from nanoindentation experiments, divided by the average density of the coatings interpolated from the values of the pure fcc-TiN, fcc-AlN and fcc-TaN by applying a rule of mixture, resulting in 331.5 m/s for fcc-Ti_{1-x}Al_xN and 216.1 m/s for 23 at.% of Ta. The calculated values for the thermal conductivity, with 9.25 W/(mK) for 0 at.% Ta and 5.22 W/(mK) for 23 at.% of Ta, are for all coatings higher than the values obtained by the TDTR measurements, as shown in Fig. 4. However, the decrease of the thermal conductivity with increasing Ta content is consistent with the experiment. The higher estimated values compared to the measured ones, suggest that other phonon scattering processes diminish the thermal conductivity more effectively. On the one hand, phonon-phonon scattering processes have been neglected on defining a ballistic transport, which can be a reason for higher calculated values. On the other hand, the incorporation of Al into the fcc-TiN lattice and the incorporation of the large Ta atoms into the fcc-Ti_{1-x}Al_xN crystal can also reduce the thermal conductivity by causing lattice distortion and generating local strain fields, that decrease the local mean free path of the phonons [25]. This phenomenon is also known as alloy scattering. As Ta is a heavy element, the alloy scattering and the disarranging of the vibration modes is pronounced even at small amounts of Ta [51,52]. When dealing with different sources of scattering, the Matthiessen's rule can be applied to

combine the different influences to get the phonon relaxation time. There, the challenging factor to evaluate the thermal conductivity is to obtain the correct scattering rates caused by the different atoms composing the alloys [25]. Summarizing, to reliably estimate the thermal conductivity, numerical simulations are required, which is out of the scope of the present work [25,51,52]. From the present study it can be assumed that the addition of Ta to the fcc-Ti_{1-x}Al_xN coating system results in a decrease of the thermal conductivity due to the combination of boundary scattering and increased alloy scattering and therefore may contribute to an enhanced tool lifetime [25,53].

4. Conclusion

Single phase face-centered cubic (fcc)-Ti_{1-x-y}Al_xTa_yN coatings with a Ti/Al ratio of 1:1 and Ta contents from 0 up to 23 at.% have been deposited by cathodic arc evaporation on cemented carbide substrates and the thermal conductivity has been determined by time-domain thermoreflectance. In comparison to fcc-TiN, the fcc-Ti_{1-x}Al_xN coating exhibited a significantly reduced thermal conductivity, as a result of phonon alloy scattering due incorporation of Al into the fcc-TiN lattice. With systematically increasing Ta content, the thermal conductivity was further decreased, reaching a minimum of one third of its initial value, as a consequence of even more intense alloy scattering due to the additionally incorporated Ta atoms and a significantly reduced grain size. The results gained within this study provide the basis for a tailored thermal conductivity of fcc-Ti_{1-x}Al_xN based hard coatings by the targeted selection of the Ta content.

CRedit authorship contribution statement

Helene Waldl: Conceptualization, Methodology, Investigation, Validation, Formal analysis, Writing - original draft, Visualization. **Michael Tkadletz:** Methodology, Investigation, Validation, Writing - review & editing, Supervision. **Markus Winkler:** Investigation, Methodology. **Birgit Grossmann:** Investigation, Methodology. **Christoph Czettl:** Resources, Funding acquisition. **Markus Pohler:** Resources, Funding acquisition. **Nina Schalk:** Writing - review & editing, Methodology, Supervision, Project administration, Funding acquisition.

Declaration of competing interest

The authors declare that they have no known competing financial interests or personal relationships that could have appeared to influence the work reported in this paper.

Acknowledgments

The authors want to thank Bernhard Sartory and Dr. Jaroslaw Wosik (Materials Center Leoben) for the FIB and SEM work. The financial support by the Austrian Federal Ministry for Digital and Economic Affairs and the National Foundation for Research, Technology and Development is gratefully acknowledged. This work was supported by the Österreichische Forschungsförderungsgesellschaft FFG (grant number 845255).

References

- [1] O. Knotek, M. Böhmer, T. Leyendecker, On structure and properties of sputtered Ti and Al based hard compound films, *J. Vac. Sci. Technol. A Vacuum, Surfaces, Film.* 4 (1986) 2695–2700, <https://doi.org/10.1116/1.573708>.
- [2] W. Münz, Titanium aluminum nitride films: a new alternative to TiN coatings, *J. Vac. Sci. Technol. A Vacuum, Surfaces, Film.* 4 (1986) 2717–2725, <https://doi.org/10.1116/1.573713>.
- [3] A. Hörling, L. Hultman, M. Odén, J. Sjölen, L. Karlsson, Mechanical properties and machining performance of Ti_{1-x}Al_xN-coated cutting tools, *Surf. Coatings Technol.* 191 (2005) 384–392, <https://doi.org/10.1016/J.SURFCOAT.2004.04.056>.

- [4] A. Kimura, H. Hasegawa, K. Yamada, T. Suzuki, Effects of Al content on hardness, lattice parameter and microstructure of $Ti_{1-x}Al_xN$ films, *Surf. Coatings Technol.* 120–121 (1999) 438–441, [https://doi.org/10.1016/S0257-8972\(99\)00491-0](https://doi.org/10.1016/S0257-8972(99)00491-0).
- [5] E. Pflüger, A. Schröer, P. Voumard, W.-D. Münz, Influence of incorporation of Cr and Y on the wear performance of TiAlN coatings at elevated temperatures, *Surf. Coatings Technol.* 115 (1999) 17–23, [https://doi.org/10.1016/S0257-8972\(99\)00059-6](https://doi.org/10.1016/S0257-8972(99)00059-6).
- [6] H. Riedl, D. Holec, R. Rachbauer, P. Polcik, R. Hollerweger, J. Paulitsch, P. H. Mayrhofer, Phase stability, mechanical properties and thermal stability of Y alloyed Ti–Al–N coatings, *Surf. Coatings Technol.* 235 (2013) 174–180, <https://doi.org/10.1016/J.SURFcoat.2013.07.030>.
- [7] M. Pfeiler, K. Kutschej, M. Penoy, C. Michotte, C. Mitterer, M. Kathrein, The influence of bias voltage on structure and mechanical/tribological properties of arc evaporated Ti–Al–V–N coatings, *Surf. Coatings Technol.* (2007), <https://doi.org/10.1016/j.surfcoat.2007.07.045>.
- [8] R. Hollerweger, H. Riedl, J. Paulitsch, M. Arndt, R. Rachbauer, P. Polcik, S. Primig, P.H. Mayrhofer, Origin of high temperature oxidation resistance of Ti–Al–Ta–N coatings, *Surf. Coatings Technol.* 257 (2014) 78–86, <https://doi.org/10.1016/J.SURFcoat.2014.02.067>.
- [9] C.M. Koller, R. Hollerweger, C. Sabitzer, R. Rachbauer, S. Kolozsvári, J. Paulitsch, P.H. Mayrhofer, Thermal stability and oxidation resistance of arc evaporated TiAlN, TaAlN, TiAlTaN, and TiAlN/TaAlN coatings, *Surf. Coatings Technol.* 259 (2014) 599–607, <https://doi.org/10.1016/j.surfcoat.2014.10.024>.
- [10] M. Pfeiler, C. Scheu, H. Hutter, J. Schnöller, C. Michotte, C. Mitterer, M. Kathrein, On the effect of Ta on improved oxidation resistance of Ti–Al–Ta–N coatings, *J. Vac. Sci. Technol. A Vacuum, Surfaces, Film.* 27 (2009) 554–560, <https://doi.org/10.1116/1.3119671>.
- [11] X. Sui, G. Li, C. Jiang, H. Yu, K. Wang, Q. Wang, Effect of Ta content on microstructure, hardness and oxidation resistance of TiAlTaN coatings, *Int. J. Refract. Met. Hard Mater.* 58 (2016) 152–156, <https://doi.org/10.1016/J.IJRMHM.2016.04.014>.
- [12] W.M. Seidl, M. Bartosik, S. Kolozsvári, H. Bolvardi, P.H. Mayrhofer, Improved mechanical properties, thermal stabilities, and oxidation resistance of arc evaporated Ti–Al–N coatings through alloying with Ta, *Surf. Coatings Technol.* 344 (2018) 244–249, <https://doi.org/10.1016/J.SURFcoat.2018.03.014>.
- [13] B. Grossmann, A. Jamnig, N. Schalk, C. Czettl, M. Pohler, C. Mitterer, Tailoring age hardening of $Ti_{1-x}Al_xN$ by Ta alloying, *J. Vac. Sci. Technol. A Vacuum, Surfaces, Film.* 35 (2017) 060604, <https://doi.org/10.1116/1.4995000>.
- [14] B. Grossmann, M. Tkadletz, N. Schalk, C. Czettl, M. Pohler, C. Mitterer, High-temperature tribology and oxidation of $Ti_{1-x-y}Al_xTa_yN$ hard coatings, *Surf. Coatings Technol.* 342 (2018) 190–197, <https://doi.org/10.1016/J.SURFcoat.2018.02.062>.
- [15] R. Rachbauer, D. Holec, P.H. Mayrhofer, Increased thermal stability of Ti–Al–N thin films by Ta alloying, *Surf. Coatings Technol.* 211 (2012) 98–103, <https://doi.org/10.1016/J.SURFcoat.2011.07.009>.
- [16] M. Bartosik, H.J. Böhm, C. Krywka, Z.L. Zhang, P.H. Mayrhofer, Influence of phase transformation on the damage tolerance of Ti–Al–N coatings, *Vacuum* 155 (2018) 153–157, <https://doi.org/10.1016/j.vacuum.2018.06.001>.
- [17] Y. Yang, Y.X. Xu, L. Chen, P.H. Mayrhofer, Improved Ti–Al–N coatings through Ta alloying and multilayer architecture, *Surf. Coatings Technol.* 328 (2017) 428–435, <https://doi.org/10.1016/J.SURFcoat.2017.09.016>.
- [18] C.M. Koller, S.A. Glatz, H. Riedl, S. Kolozsvári, P. Polcik, H. Bolvardi, P. H. Mayrhofer, Structure and mechanical properties of architecturally designed Ti–Al–N and Ti–Al–Ta–N-based multilayers, *Surf. Coatings Technol.* 385 (2020), 125355, <https://doi.org/10.1016/J.SURFcoat.2020.125355>.
- [19] G. List, G. Sutter, A. Bouthiche, Cutting temperature prediction in high speed machining by numerical modelling of chip formation and its dependence with crater wear, *Int. J. Mach. Tools Manuf.* (2012), <https://doi.org/10.1016/j.ijmachtools.2011.11.009>.
- [20] I. Krajinović, W. Daves, M. Tkadletz, T. Tepperneegg, T. Klünsner, N. Schalk, C. Mitterer, C. Tritremmel, W. Ecker, C. Czettl, Finite element study of the influence of hard coatings on hard metal tool loading during milling, *Surf. Coatings Technol.* 304 (2016) 134–141, <https://doi.org/10.1016/J.SURFcoat.2016.06.041>.
- [21] M. Tkadletz, N. Schalk, R. Daniel, J. Keckes, C. Czettl, C. Mitterer, Advanced characterization methods for wear resistant hard coatings: a review on recent progress, *Surf. Coatings Technol.* 285 (2016) 31–46, <https://doi.org/10.1016/J.SURFcoat.2015.11.016>.
- [22] L. Braginsky, A. Gusarov, V. Shklover, Models of thermal conductivity of multilayer wear resistant coatings, *Surf. Coatings Technol.* (2009), <https://doi.org/10.1016/j.surfcoat.2009.08.052>.
- [23] A.W. Nemetz, W. Daves, T. Klünsner, W. Ecker, T. Tepperneegg, C. Czettl, I. Krajinović, FE temperature- and residual stress prediction in milling inserts and correlation with experimentally observed damage mechanisms, *J. Mater. Process. Technol.* (2018), <https://doi.org/10.1016/j.jmatprotec.2018.01.039>.
- [24] V. Moraes, H. Riedl, R. Rachbauer, S. Kolozsvári, M. Ikeda, L. Prochaska, S. Paschen, P.H. Mayrhofer, Thermal conductivity and mechanical properties of AlN-based thin films, *J. Appl. Phys.* 119 (2016), <https://doi.org/10.1063/1.4953358>.
- [25] T. Hori, J. Shiomi, Tuning phonon transport spectrum for better thermoelectric materials, *Sci. Technol. Adv. Mater.* 20 (2019) 10–25, <https://doi.org/10.1080/14686996.2018.1548884>.
- [26] W. Kalss, A. Reiter, V. Derflinger, C. Gey, J.L. Endrino, Modern coatings in high performance cutting applications, *Int. J. Refract. Met. Hard Mater.* 24 (2006) 399–404, <https://doi.org/10.1016/j.ijrmhm.2005.11.005>.
- [27] X.Z. Ding, M.K. Samani, G. Chen, Thermal conductivity of PVD TiAlN films using pulsed photothermal reflectance technique, *Appl. Phys. A Mater. Sci. Process.* 101 (2010) 573–577, <https://doi.org/10.1007/s00339-010-5900-0>.
- [28] M.K. Samani, G.C.K. Chen, X.Z. Ding, X.T. Zeng, Thermal conductivity of CrAlN and TiAlN coatings deposited by lateral rotating cathode arc, *Key Eng. Mater.* 447 (2010) 705–709, <https://doi.org/10.4028/www.scientific.net/KEM.447-448.705>.
- [29] R. Rachbauer, J.J. Gengler, A.A. Voevodin, K. Resch, P.H. Mayrhofer, Temperature driven evolution of thermal, electrical, and optical properties of Ti–Al–N coatings, *Acta Mater.* (2012), <https://doi.org/10.1016/j.actamat.2012.01.005>.
- [30] G.S. Fox-Rabinovich, K. Yamamoto, M.H. Aguirre, D.G. Cahill, S.C. Veldhuis, A. Biksa, G. Dosbaeva, L.S. Shuster, Multi-functional nano-multilayered AlTiN/Cu PVD coating for machining of Inconel 718 superalloy, *Surf. Coatings Technol.* 204 (2010) 2465–2471, <https://doi.org/10.1016/J.SURFcoat.2010.01.024>.
- [31] NIST 660c certificate, (n.d.). <https://www-s.nist.gov>.
- [32] U. Welzel, J. Ligot, P. Lamparter, A.C. Vermeulen, E.J. Mittemeijer, Stress analysis of polycrystalline thin films and surface regions by X-ray diffraction, *J. Appl. Crystallogr.* 38 (2005) 1–29, <https://doi.org/10.1107/S0021889804029516>.
- [33] D.G. Cahill, Analysis of heat flow in layered structures for time-domain thermoreflectance, *Rev. Sci. Instrum.* 75 (2004) 5119–5122, <https://doi.org/10.1063/1.1819431>.
- [34] A.O. Eriksson, J.Q. Zhu, N. Ghafoor, M.P. Johansson, J. Sjölen, J. Jensen, M. Odén, L. Hultman, J. Rosén, Layer formation by resputtering in Ti–Si–C hard coatings during large scale cathodic arc deposition, *Surf. Coatings Technol.* 205 (2011) 3923–3930, <https://doi.org/10.1016/j.surfcoat.2011.02.007>.
- [35] R. Aninat, N. Valle, J.-B. Chemin, D. Duday, C. Michotte, M. Penoy, L. Bourgeois, P. Choquet, Addition of Ta and Y in a hard Ti–Al–N PVD coating: individual and conjugated effect on the oxidation and wear properties, *Corros. Sci.* 156 (2019) 171–180, <https://doi.org/10.1016/j.corsci.2019.04.042>.
- [36] H. Oettel, R. Wiedemann, Residual stresses in PVD hard coatings, *Surf. Coatings Technol.* 76–77 (1995) 265–273, [https://doi.org/10.1016/0257-8972\(95\)02581-2](https://doi.org/10.1016/0257-8972(95)02581-2).
- [37] R. Rachbauer, D. Holec, P.H. Mayrhofer, Phase stability and decomposition products of Ti–Al–Ta–N thin films, *Appl. Phys. Lett.* 97 (2010) 3–5, <https://doi.org/10.1063/1.3495783>.
- [38] P. Scherrer, *Bestimmung der Grosse und der inneren Struktur von Kolloidteilchen mittels Röntgenstrahlen*, *Nachrichten von Der Gesellschaft Der Wissenschaften Zu Göttingen, Math. Klasse.* (1918) 98–100.
- [39] G.K. Williamson, W.H. Hall, X-ray line broadening from filed aluminium and wolfram, *Acta Metall.* 1 (1953) 22–31, [https://doi.org/10.1016/0001-6160\(53\)90006-6](https://doi.org/10.1016/0001-6160(53)90006-6).
- [40] T. Ungár, G. Tichy, J. Gubicza, R.J. Hellmig, Correlation between subgrains and coherently scattering domains, *Powder Diffract.* 20 (2005) 366–375, <https://doi.org/10.1154/1.2135313>.
- [41] M. Tkadletz, A. Lechner, N. Schalk, B. Sartory, M. Winkler, C. Mitterer, Reactively sputtered TiN/SiO₂ multilayer coatings with designed anisotropic thermal conductivity – from theoretical conceptualization to experimental validation, *Surf. Coatings Technol.* 393 (2020), 125763, <https://doi.org/10.1016/j.surfcoat.2020.125763>.
- [42] M.W. Chase, NIST-JANAF thermochemical tables: fourth edition, *J. Phys. Chem. Ref. Data* 9 (1998) 1–1951.
- [43] A. Petit, P.-L. Dulong, *Recherches sur quelques points importants de la Théorie de la Chaleur*, *Ann. Chim. Phys.* 10 (1819) 395–413.
- [44] W. Martienssen, H. Warlimont, *Condensed Matter and Materials Data*, Springer Berlin Heidelberg New York, 2011, <https://doi.org/10.1007/s13398-014-0173-7.2>.
- [45] M.K. Samani, X.Z. Ding, S. Amini, N. Khosravian, J.Y. Cheong, G. Chen, B.K. Tay, Thermal conductivity of titanium aluminum silicon nitride coatings deposited by lateral rotating cathode arc, *Thin Solid Films* 537 (2013) 108–112, <https://doi.org/10.1016/j.tsf.2013.04.029>.
- [46] A. Jacquot, B. Lenoir, A. Dauscher, P. Verardi, F. Craciun, M. Stölzer, M. Gartner, M. Dinescu, Optical and thermal characterization of AlN thin films deposited by pulsed laser deposition, *Appl. Surf. Sci.* 186 (2002) 507–512, [https://doi.org/10.1016/S0169-4332\(01\)00767-X](https://doi.org/10.1016/S0169-4332(01)00767-X).
- [47] M. Hans, D. Music, Y.T. Chen, L. Patterer, A.O. Eriksson, D. Kurapov, J. Ramm, M. Arndt, H. Rudigier, J.M. Schneider, Crystallite size-dependent metastable phase formation of TiAlN coatings, *Sci. Rep.* 7 (2017) 1–7, <https://doi.org/10.1038/s41598-017-16567-z>.
- [48] S. Lee, J. Lee, Compositionally gradient ($Ti_{1-x}Al_x$)N coatings made by plasma enhanced chemical vapor deposition, *J. Vac. Sci. Technol. A Vacuum, Surfaces, Film.* 13 (1995) 2030–2034, <https://doi.org/10.1116/1.579648>.
- [49] T. Hori, J. Shiomi, C. Dames, Effective phonon mean free path in polycrystalline nanostructures, *Appl. Phys. Lett.* 106 (2015) 10–15, <https://doi.org/10.1063/1.4918703>.
- [50] T. Feng, X. Ruan, Prediction of spectral phonon mean free path and thermal conductivity with applications to thermoelectrics and thermal management: a review, *J. Nanomater.* 2014 (2014), <https://doi.org/10.1155/2014/206370>.

- [51] Z. Tian, S. Lee, G. Chen, Comprehensive review of heat transfer in thermoelectric materials and devices, *Annu. Rev. Heat Transf.* 17 (2014) 425–483, <https://doi.org/10.1615/annualrevheattransfer.2014006932>.
- [52] A. Kundu, N. Mingo, D.A. Broido, D.A. Stewart, Role of light and heavy embedded nanoparticles on the thermal conductivity of SiGe alloys, *Phys. Rev. B - Condens. Matter Mater. Phys.* 84 (2011) 1–5, <https://doi.org/10.1103/PhysRevB.84.125426>.
- [53] K. Biswas, J. He, I.D. Blum, C.I. Wu, T.P. Hogan, D.N. Seidman, V.P. Dravid, M. G. Kanatzidis, High-performance bulk thermoelectrics with all-scale hierarchical architectures, *Nature* 489 (2012) 414–418, <https://doi.org/10.1038/nature11439>.